Effect of Antenna Aperture Field on Co-channel Interference, Capacity, and Payload Mass in High Altitude Platform Communications

John Thornton and David Grace

In a High Altitude Platform (HAP) cellular communications network, each cell may be served by a dedicated spot-beam antenna. The antennas' beam properties and their spatial overlap control the co-channel interference. In prior literature, radiation patterns have been approximated by a main lobe followed by a constant sidelobe floor. A network of 121 cells has been studied and the method is here extended to the use of more realistic radiation patterns based on the theoretical aperture antenna patterns. This allows for the comparison of the effect of different aperture field tapers, which lead to reduced sidelobe levels and hence higher system capacity but also a more massive antenna payload.

Keywords: High Altitude Platforms, antennas, cellular communications, carrier-to-interference ratio.

I. Introduction

1. Background

High altitude platforms (HAPs) — aircraft or lighter-than-air platforms stationed in the stratosphere — are gaining interest as a possible means of supporting wireless telecommunications services [1], [2]. They will allow for line-of-sight links, which may be a particularly effective means of exploiting the high bandwidths available at mm-wave frequencies by using multi-

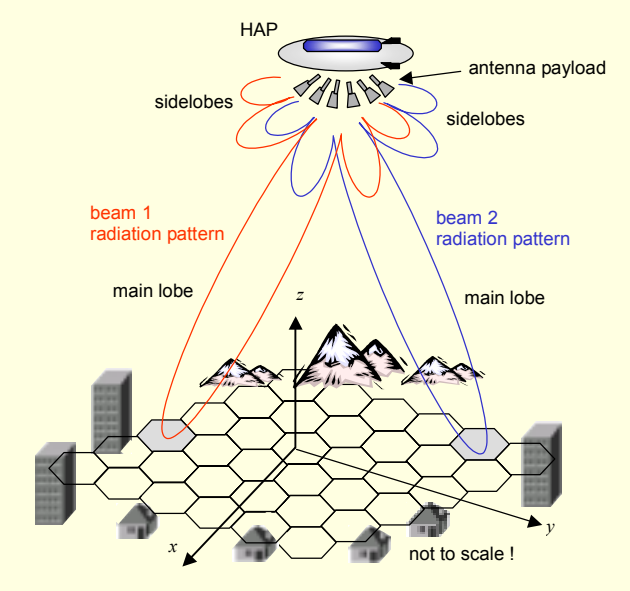

Fig. 1. Overlapping spot-beams serving co-channel cells in HAPs communications.

Manuscript received Jan. 20, 2004; revised June 3, 2004.

John Thornton (phone: + 44 1904 433248, email: jt21@ohm.york.ac.uk) and David Grace (email: dg@ohm.york.ac.uk) are with the Communications Research Group, Department of Electronics, University of York, UK.

cell architectures [3], [4].

Each cell may be served by a dedicated spot-beam antenna. The antenna payload may comprise one antenna per cell or employ multiple-beam antennas such as lens or reflector antennas with multiple feeds. The important feature is that the cellular network allows for the spatial re-use of spectrum and thus has high spectral efficiency. This spectral efficiency tends to increase as cell sizes are reduced and their numbers increased until the additional interference limits the total capacity.

The level of carrier-to-interference ratio (CIR) in a HAP cellular network, assuming line-of-sight links, is a consequence of spatial spectrum re-use and is dominated by the antenna radiation patterns. The geometry is illustrated in Fig. 1, where just two co-channel beams are shown. Each beam comprises a main lobe, which is directed towards the cell it is serving, and a sidelobe region which contributes interference to other cells. It is the form of the sidelobe region which is of particular interest in this paper.

For a given co-channel cell group, and given knowledge of each radiation pattern, the CIR at each ground position (x, y) can be calculated from [5]:

$$\mathbf{CIR}(x,y) = \frac{P_{\max}(x,y)}{\left(\sum_{i=1}^{n} P_i(x,y)\right) - P_{\max}(x,y)}, \quad (1)$$

where $P_{\max}(x, y)$ is the maximum power of a beam from a set of n co-channel beams and is therefore defined as the carrier (the wanted signal). The denominator in (1) is the sum of the powers in all the other beams, which is the aggregate interference. Before (1) can be evaluated, it is necessary to define both a radiation pattern for each cell's antenna, and an antenna pointing angle, so that the power on the ground $P(x, y)$ can be evaluated for each beam. We previously reported the methodology in [5], and rather than repeat this we will list the key features:

- A layout of equal-size hexagonal cells was used to allow cell tessellation.
- A method for systematically deriving each antenna beamwidth and pointing angle was developed. This aided an iterative approach for calculating each power footprint in software.
- For each cell, the antenna azimuth and elevation beamwidths were chosen to optimize power at the cell edge[1)], leading to circular power contours and generally asymmetric beams.
- Having specified each beamwidth, the main lobe was modeled as a simple curve where power rolled-off with angle at a rate controlled by a single parameter.
- Beyond a certain main lobe power roll-off, a flat sidelobe region was assumed, typically at 40 dB below the maximum gain.
- CIR levels were presented as contour plots and as area distribution plots.
- A network of 121 cells covering a 60 km coverage circle was used.
- CIR distributions for channel re-use numbers of 3, 4, and 7 were compared.

The importance of minimizing the average sidelobe level was identified. The figure of -40 dB is realistic for a carefully designed lens antenna operating at a carrier frequency of around 30 GHz, such as the asymmetric beam lens antenna of [7]. We also suggested that, in a system of many beams, the structure of the sidelobe region is rather less important than its mean level. The latter assumption is of course open to question, and in this work the effect of the shape of the sidelobe region is studied. This paper describes how a system of many co-channel antenna beams may be modeled by deriving for each beam the theoretical radiation pattern based on the aperture electrical size and field distribution. This presents an advancement beyond the rather simplistic flat sidelobe model of [5] and also leads to insight into the relationship between antenna payload size and co-channel interference.

2. Organization of the Paper

It is well known that the electric field amplitude taper in the aperture of the antenna controls the radiation pattern and the sidelobe level. Using a convenient expression for radial amplitude distribution in the aperture, we quantify both the reduction in sidelobe levels and the associated reduction in directivity. We then derive terms to quantify by how much the aperture diameter needs to be scaled to attain a given directivity. For each cell, the required directivity is dictated by the size of the cell and its geometry with respect to the HAP. Using a conventional cellular layout of contiguous, equal-size hexagons leads to a requirement for more distant cells to be illuminated by antennas of greater directivity.

Whereas our earlier work [5] used a flat sidelobe model, we show how the revised model for aperture radiation patterns leads to modified results for CIR distribution. We go on to estimate bandwidth efficiency based on practical modulation schemes. This ultimately leads to a model that allows us to consider the trade-off between antenna payload size and the network data capacity.

1) This choice of beamwidth is in contrast to a common assumption that the half power beamwidth corresponds to the cell edge, e.g. [6].

II. Methodology for Aperture Antenna Radiation Patterns

The antenna radiation pattern in the far field can be computed from the transform of the aperture field. This may be expressed as a two dimensional integration over the aperture surface. For a circular aperture, the far field is given by [8]:

$$E(\theta,\phi)=\int_{\phi'=0}^{2\pi}\int_{r=0}^{1}A(r,\phi')\exp\left(j\,k\sin\theta\;r\,a\cos(\phi-\phi')\right)r\,dr\,d\phi', \tag{2}$$

where the aperture distribution, $A(r,\phi')$, is in general a function of normalized radius r and angle ϕ', as shown in Fig. 2.

For a circularly symmetric aperture distribution, such as occurs with a cylindrical corrugated horn [9], there is no ϕ' dependency, and the distribution is thus expressed as $A(r)$. In this case the far field is also circularly symmetric. (Note that θ and ϕ—without prime—are used to denote angular co-ordinates in the far field.) We then introduce functions for $A(r)$ to investigate the far field and, in particular, the shape of the main lobe and associated sidelobe region.

A convenient approach for various radial aperture tapers is given by [10]:

$$A(r)=\left(1-r^2\right)^p, \tag{3}$$

where $A(r)$ is real, and where p controls the rate of roll-off of the E-field amplitude. This approach is useful because the far field in (2) has an analytical solution given by:

$$E(\theta)=\frac{\pi R^2\;2^p\;p!\;J_{p+1}(u)}{u^{p+1}}, \tag{4}$$

where

$$u=k\,R\,\sin\theta, \tag{5}$$

R is the aperture radius, and k is the wavenumber ($=2\pi/\lambda$ where λ is wavelength). Thus, the far field may be derived for each angle θ using (4) rather than using the more computationally intensive numerical solution of (2). This allows for the calculation of each antenna's radiation pattern based on a single parameter, p, and this later helps us to compare the properties of different HAP antenna payloads based on this parameter. To illustrate the form of (4), the radiation patterns for a circular aperture having a radius of 5 wavelengths, and for various amplitude tapers p, are shown in Fig. 3. The case for p=0 is, of course, that for a uniformly illuminated aperture.

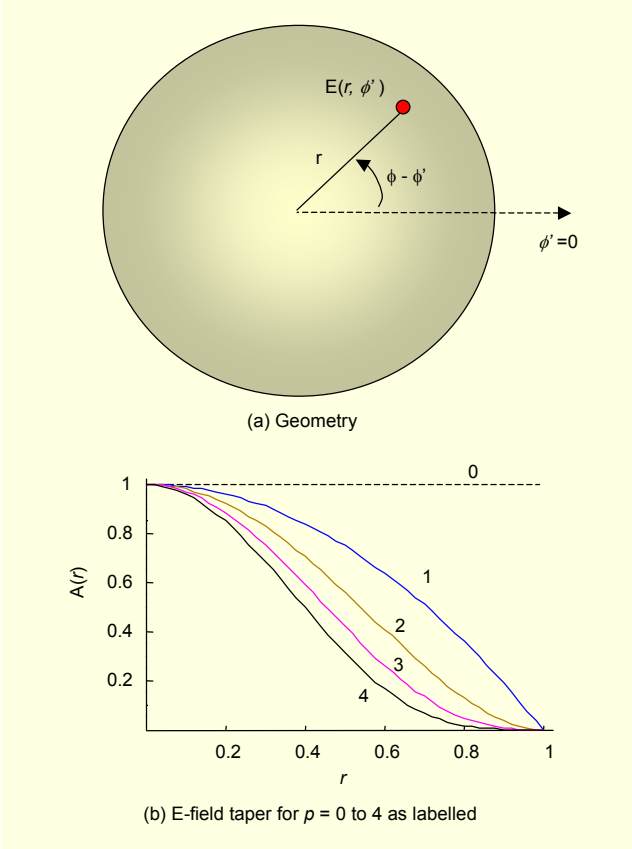

Fig. 2. E-field distribution for a circular aperture.

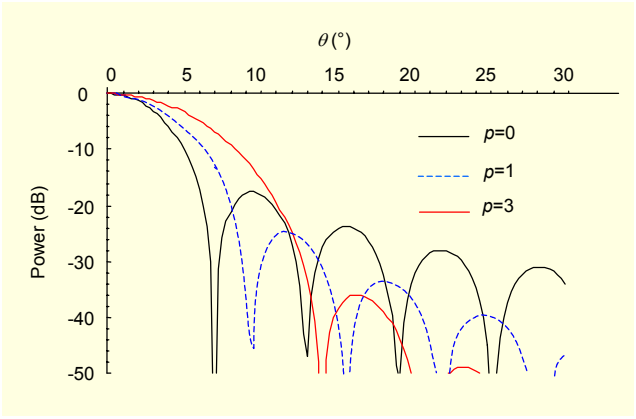

Fig. 3. Normalized radiation patterns for a fixed diameter circular aperture with various amplitude tapers.

In Fig. 3 the power values are normalized. It is apparent that as p increases, the main lobe becomes wider, and the sidelobe levels reduce. The main lobe widening leads to a reduction in directivity, and the maximum directivity D (at $\theta=0$) can in each case be approximated from the main lobe half-power beamwidth (HPBW) using the Kraus approximation:

$$D=\frac{4\pi}{\mathrm{HPBW}^2}. \tag{6}$$

III. Implications of the Aperture Function for the HAP Antenna Payload

Where sidelobe levels are reduced by the use of an amplitude taper, the associated loss in directivity must be countered by increasing the aperture diameter to produce the required beamwidth, which is dictated by the size and location of each cell. The increase in diameter would lead to an increase in antenna mass. The following sections explore these effects for a system of many cells, and thus require a fairly generalized approach.

First, a relationship is sought between aperture taper term p and the aperture diameter required to achieve a given beamwidth. This has been investigated using software to derive the directivity from the HPBW of the patterns of the type shown in Fig. 3 for many values of diameter and for several values of p. In each case, the directivity is compared to that for a uniform aperture (p=0) to derive the reduction in directivity associated with taper term p. The results are shown in Fig. 4, where it is apparent that the directivity reduction is more or less constant with diameter. This allows for a convenient way of choosing the required combination of aperture diameter and taper p to yield a wide range of HPBWs, i.e., for any cell within the HAP coverage area.

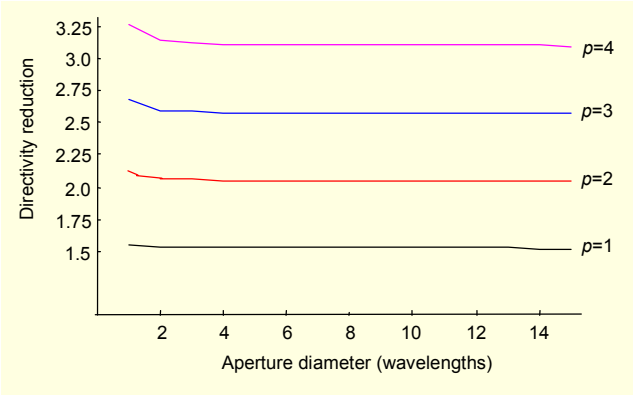

Fig. 4. Loss in directivity, compared to a uniform aperture, associated with the aperture amplitude taper.

Table 1. Directivity reduction and required aperture scaling terms, for given taper p.

Taper term p	Directivity reduction	Required aperture scaling term
1	1.52 (1.8 dB)	$\sqrt{1.52}$
2	2.05 (3.1 dB)	$\sqrt{2.05}$
3	2.6 (4.1 dB)	$\sqrt{2.6}$
4	3.1 (4.9 dB)	$\sqrt{3.1}$

From Fig. 4. the nearly-constant terms for directivity reduction, compared to the uniform aperture (p=0), are summarized in Table 1 below.

The methodology for generating the theoretical radiation patterns, along with the associated sidelobes, can now be summarized:

i) Use the established method [5] to calculate the required antenna HPBWs for each cell, based on the cell subtended angles.

ii) Use an established approximation which relates aperture diameter to HPBW (given in degrees) for a uniform aperture [8]:

$$\text{diameter} \approx \frac{60\,\lambda}{\text{HPBW}}.$$

iii) For a chosen value of p, use Table 1 to derive the new required aperture diameter.

iv) Use (4) to model the radiation pattern for each antenna, based on aperture diameter and the chosen value of p.

v) Compute the CIR for the group of all co-channel beams, as for the established method [5].

The CIR may be calculated at each ground position within the HAP coverage area using the above method for generating the radiation patterns. We thus have a method for generating a more informative sidelobe structure than the "flat sidelobe floor" approach which has been previously used and reported. This allows us to choose a taper term p to reduce sidelobes compared to a uniform aperture, and to use Table 1 to estimate the associated required increase in antenna dimensions.

IV. Results for Carrier-to-Interference Ratio

1. Uniform Apertures

To illustrate the approach for the derivation of radiation patterns, Fig. 5 shows the power footprints of the antennas serving (a) the central cell, and (b) a distant cell in the outer ring, where a uniform aperture is used in each case (i.e., p=0). This yields the worst-case sidelobe levels, but also the smallest antenna aperture. The HAP is placed at a height of 17 km above the centre of the coverage area. The term "footprint" refers to the apparent directivity of the antenna at each point on the ground, so it represents points on a cartesian plane which intersects the radiation pattern.

In Fig. 5 the sidelobe periodicity is greater for case (b) than for case (a) because the antenna serving the more distant cell (b) has a larger aperture diameter. Also, the beams are asymmetric in order to produce circular cell footprints. The three-dimensional pattern for an elliptic aperture may be

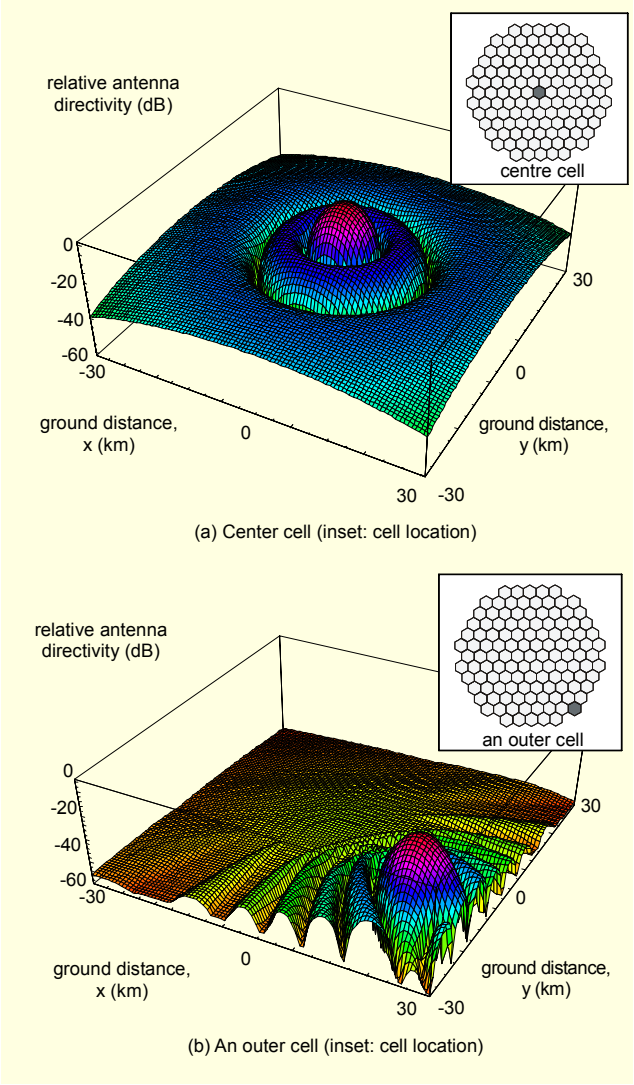

Fig. 5. Cartesian plots of an aperture antenna radiation pattern.

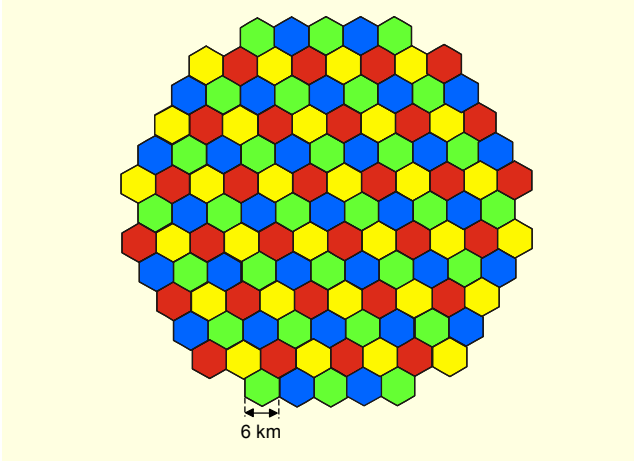

Fig. 6. Layout for 121 cells, showing a 4 channel re-use plan.

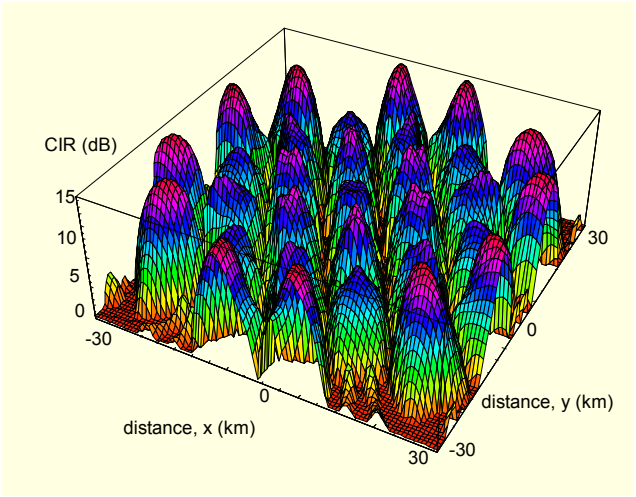

Fig. 7. The CIR distribution for aperture antenna model, p=0 (uniform aperture).

synthesized from the patterns of two circular apertures, i.e., interpolating between the narrow beam case and the wider beam case. The validity of this approach, i.e., interpolating between two two-dimensional patterns, has been verified by comparison with a rigorous numerical derivation of the pattern of an elliptic aperture, where the taper term (2) applies along both the major and minor ellipse axes (the rigorous numerical method involves many more computational steps, and while this is not problematic for deriving a single antenna radiation pattern, it is somewhat intractable for simulating the CIR in a network of many co-channel beams, which are in general dissimilar and whose patterns must be derived for each cell).

Retaining the cellular layout of 121 cells covering a 60 km diameter region, the 4 channel re-use plan is illustrated in Fig. 6 where the cells on the same channel are represented by one of four colours. For one of these groups of co-channel cells (the blue cells, of which there are 31), the calculated CIR levels arising from co-channel interference for all antenna beams is shown in Fig. 7.

In Fig. 7(where, for clarity, CIR values have been truncated at 0 dB) there are 31 distinct "peaks" corresponding to the locations of the cells on this channel. The other three channels have a similar looking distribution of peaks and troughs. The distribution of CIR can be presented by plotting the fraction of the cell-group area versus the minimum CIR, which is a useful way of comparing CIR levels for different antenna types. This is presented in the next section.

2. Effect of Tapered Aperture Function on CIR

The effect of a non-zero aperture taper term p (and, consequently, increased antenna aperture diameters) is investigated next. Figure 8 shows theoretical radiation patterns

using values of p between 0 and 3. In contrast to Fig. 3, the plots in Fig. 8 are for a fixed HPBW—chosen arbitrarily as 15°—and hence the aperture diameter is re-scaled for each value of p according to the third column of Table 1.

The computation of the CIR for each ground position was repeated using the above methodology. The computed CIR coverage levels, for the 31 co-channel cell group and for each of the antenna models discussed, are shown in Fig. 9. The expected trend that a higher value for p (more severe aperture taper leading to reduced sidelobes) leads to higher CIR values is apparent. The results using a flat sidelobe model have also been included for comparison.

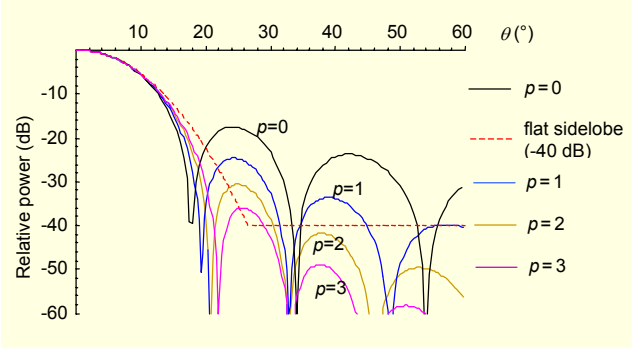

Fig. 8. Example theoretical antenna radiation patterns for increasing aperture taper p, for a fixed HPBW.

The form of the curves in Fig. 9 can be interpreted as follows: For low CIR values, e.g., less than 10 dB, all the cell-group area experiences at least this CIR. For higher CIR values, a lesser fraction of the cell group's area experiences a value greater than that shown on the x-axis. For each curve, the points at which coverage drops below 1 show the CIR experienced at some cell edges. Similarly, the points at which coverage approaches zero show the CIR levels experienced at some cell centers. It is also evident that the flat sidelobe method, although the simplest in terms of there being no sidelobe variation with angle, yields results which are similar in form to the much more detailed method that uses the theoretical radiation pattern for each aperture. The aperture model also leads to a faster main lobe roll-off than the $(\cos\theta)^n$ model of [5] and thus contributes to reduced co-channel interference for values of p greater than zero.

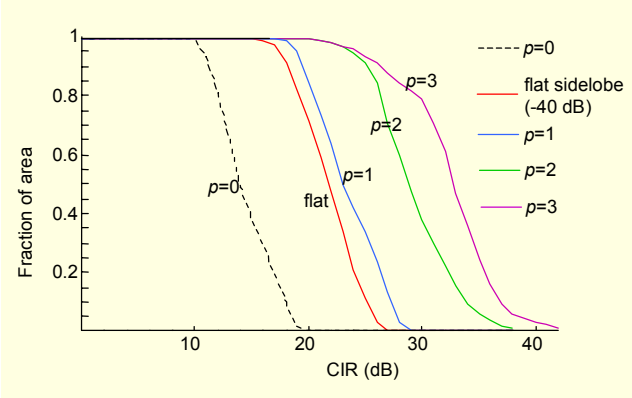

Fig. 9. CIR coverage for various aperture amplitude tapers, for 1 channel of 4.

V. Calculation of System Capacity

It remains to summarize the relationship between co-channel CIR levels, the likely minimum and maximum data capacity, and the relative size of the antenna payload.

The CIR at each point (x,y) on the ground can be converted into bandwidth efficiency using four modulation and coding schemes as shown in Table 2 [11]. Such schemes are normally used as part of an adaptive modulation and coding strategy, where the scheme delivering the highest rate commensurate with the Carrier to Interference plus Noise Ratio (CINR) is selected. One example of their use is in the IEEE 802.16 standard [12]. The CINR values shown have been determined assuming that the noise plus interference is Gaussian, and therefore this CINR is equivalent to the CIR (it is worth adding that, assuming line-of-sight links with relatively narrow beamwidth antennas, any scattering and multipath effects will be at a very low level and may thus be neglected).

Table 2. Modulation and coding figures used to determine capacity.[2)]

	64-QAM	64-QAM	16-QAM	GMSK
Code rate[3)]	1.0	0.69	0.69	0.69
BW efficiency (b/s/Hz)	4.8	3.3	2.2	0.9
Required E_b/N_0 (dB)	18.7	10.4	6.7	2.7
Aequired CINR (dB)[4)]	25.5	15.6	10.1	2.3

Of most interest are the minimum and maximum bandwidth efficiencies available across the cell; these correspond to the center and cell edges respectively. Additionally, if we take the case p=0 (the smallest antenna payload) as a baseline, we can determine the increase in bandwidth efficiency (equivalent to an increase in capacity) that can be achieved by increasing the

2) Abbreviations: QAM: quadrature amplitude modulation, GMSK: Gaussian mean shift keying, BW: bandwidth, BER: bite error rate.

3) Code rate = 0.6912 (rate 3/4 convolutional inner code and 188/204 Reed-Solomon outer code)

4) All CINR figures assume BER=10^{-5} and RF bandwidth = 25 MHz (we use roll-off factor = 0.25, therefore max symbol rate = 20 Msymbols/s)

Table 3. Summary of trade-off between antenna payload aperture area and CIR.

p	Minimum CIR			Maximum CIR			Aperture area compared to uniform apertures	Worst case mass increase
	CIR (dB)	BW efficiency (b/s/Hz)	Capacity increase	CIR (dB)	BW efficiency (b/s/Hz)	Capacity increase		
0	10	0.9	1	19	3.3	1	1	-
1	18	3.3	3.7	28	4.8	1.5	1.52	1.87
2	20	3.3	3.7	38	4.8	1.5	2.05	2.93
3	20	3.3	3.7	42	4.8	1.5	2.6	4.19

aperture taper p. These values are shown in Table 3 along with their respective CIR values. The increase in aperture area and worst case mass increase are also shown for comparison.

It is not practical to exploit fully the very high CIR values in the cell centers (up to 42 dB), which have been derived excluding thermal noise. In practice, on user links given typical hardware and link budget constraints the thermal noise will begin to dominate the CINR figure, limiting its maximum value to around 30 dB — the CINR figure is then noise limited [13]. Therefore the capacity increase is limited by the highest rate modulation scheme (64 QAM) that will operate practically on such links.

In the last column of Table 3, the "Worst case" mass increase assumes that all antenna dimensions scale with the aperture diameter, hence mass increases with the cubic power of length. This would occur (approximately) for some types of lens or reflector antennas, because the primary feed must also be made bigger in order to produce a narrower beam that yields the amplitude taper across the secondary aperture. In other antenna types, e.g., planar array antennas, the mass would increase linearly with aperture area (square power of length), as shown in the fourth column section of Table 3.

Hence, for each aperture taper term p, the CIR increases indicated are gained at the expense of a payload mass increase which would lie approximately between the values indicated in the last two columns of Table 3, depending on the antenna type used in the payload. A baseline estimate for total antenna mass can be derived given from the mass of a particular, representative item, and scaling this according to the required beamwidth for each cell. For example, we have a 150 mm aperture diameter lens-corrected horn offering 5° HPBW — representative of an outer cell of the 121 cell group — 700 g mass, and minimal aperture taper. From this benchmark we derive an aggregate antenna mass estimate of 40 kg at 28 GHz, which scales to 8 kg at 48 GHz. The figures are somewhat tentative and would of course be modified for a different antenna type, a multi-beam solution, or use of different materials.

The analysis indicates that the adoption of a $p=1$ taper profile will yield significant increases in capacity, which would fully justify the worst case mass increase. Increasing the aperture taper above $p=1$ yields higher CIR values, particularly at cell centers, but this does not increase capacity for the modulation and coding schemes chosen, and in these circumstances the resulting increase in mass cannot be justified.

VI. Conclusion

For a typical co-channel cell group of 31 cells served by a payload of aperture antennas on a HAP, the effect of the antenna aperture function on co-channel interference has been explored in a generalized way. For each cell, the required antenna beamwidths were derived from the cell's subtended angles, in the same manner as from previous work. The CIR values for uniform apertures were calculated to serve as a benchmark result, this being the case for the smallest aperture but the worst (highest) sidelobe levels.

While many aperture distributions are possible, an aperture taper term was chosen which conveniently allowed an analytical solution for the far field radiation pattern, and which also defined the E-field aperture taper as a function of a single integer variable p. This function was then applied to each antenna to reduce the sidelobe levels. This also entailed increasing each aperture diameter to recover the required beamwidths. A generalized approach was identified whereby the required increase in diameter for each aperture was found to be very nearly constant for a given aperture taper p over a wide range of required antenna beamwidths.

The scaling term applied to each antenna diameter readily allows for an estimate of the antenna payload mass relative to the case where all antennas use a uniform aperture distribution ($p=0$). As the antenna diameter increases, the antenna mass may increase with the square of the diameter (for planar antennas) or, in the extreme, with the cube of the diameter (e.g., for lens antennas where the lens and primary feed dimensions all increase). In practice, a HAP antenna payload may be

comprised of a variety of different antenna types. The method thus relates computed co-channel CIR values to an estimate of relative antenna payload mass.

A network of 121 cells was considered, where the spectrum is divided into four channels and the HAP placed 17 km above a service area of 60 km diameter. Compared to uniform apertures which yield a 19 dB maximum CIR, a 9 dB increase in CIR at cell centers may be achieved with a mass increase of between approximately 1.52 and 1.87. This increase in CIR provides an approximately commensurate increase in the capacity of the system. Further increases in CIR would be unlikely to provide any further increases in capacity because high order modulation schemes such as un-coded 64-QAM can already be supported.

There is very considerable scope to consider other cellular layouts and antenna payload geometries. The first HAPs or other aerial platforms to be deployed are likely to support, initially, either a single or small number of cells. The ultimate payload lift capability of future platforms is not yet well known, but it is anticipated that the above methodology and results will help inform system developers.

References

[1] G.M. Djuknic, J. Freidenfelds, and Y. Okunev, "Establishing Wireless Communications Services via High-Altitude Aeronautical Platforms: A Concept Whose Time Has Come ?" *IEEE Comm. Magazine,* Sept. 1997, pp. 128-35.

[2] T.C. Tozer and D. Grace, "High-Altitude Platforms for Wireless Communications," *IEE Electronics and Comm. Eng. J.,* vol. 13, June 2001, pp. 127-137.

[3] J. Thornton, D. Grace, C. Spillard, T. Konefal, and T. Tozer, "Broadband Communications from a High Altitude Platform - The European HeliNet Programme," *IEE Electronics and Comm. Eng. J.,* vol. 13, June 2001, pp. 138-144.

[4] R. Miura and M. Suzuki, "Preliminary Flight Test Program on Telecom and Broadcasting Using High Altitude Platform Stations," *Wireless Personal Comm.,* vol. 24, issue 2, 2003, pp. 341-361.

[5] J. Thornton, D. Grace, M.H. Capstick, and T.C. Tozer, "Optimising an Array of Antennas for Cellular Coverage from a High Altitude Platform," *IEEE Trans. Wireless Comm.,* vol. 2, no. 3, May 2003, pp. 484-492.

[6] B. El-Jabu and R. Steele, "Cellular Communications Using Aerial Platform," *IEEE Trans. Veh. Technol.*, vol. 50, no. 3, May 2001, pp. 686-700.

[7] J. Thornton, "A Low Sidelobe Asymmetric Beam Antenna for High Altitude Platform Communications," *IEEE Microwave and Wireless Components Lett.*, vol. 14, no. 2, Feb. 2004, pp.59-61.

[8] C.A. Balanis, *Antenna Theory, Analysis and Design*, 2nd ed.,Wiley, 1997.

[9] A.D. Olver, P.J.B. Clarricoats, A.A. Kishk, and L. Shafai, *Microwave Horns and Feeds*: IEE Press, 1994, pp. 266.

[10] S. Silver, *Microwave Antenna Theory and Design*, Peter Peregrinus Ltd., 1984, pp. 194.

[11] D. Grace, G. Chen, G.P. White, J. Thornton, and T.C. Tozer, "Improving the System Capacity of mm-Wave Broadband Services Using Multiple High Altitude Platforms," *Proc. IEEE Global Comm. Conf. (GLOBECOM)*, San Francisco, USA, Dec. 2003.

[12] IEEE Std. 802.16 Part 16, *Air Interface for Fixed Broadband Wireless Access Systems*, IEEE, Piscataway, N.J., Dec. 2001.

[13] D. Grace, J. Thornton, T. Konefal, C. Spillard, and T.C. Tozer, *Broadband Communications from High Altitude Platforms - The HeliNet Solution*, Invited Paper for Wireless Personal Mobile Conf., Aalborg, Denmark, vol.1, Sept. 2001, pp. 75-80.

John Thornton is a Physics Graduate of the University of York, UK, obtained the MSc. in microwave physics from the University of Portsmouth, UK, in 1995 and the PhD from the UK's Open University in 2002. He has held research posts at the Rutherford Appleton Laboratory, UK, developing sub-millimeter wave solid state sources and receivers, and at the University of Oxford, on projects including passive radar transponders, array antennas and superconducting filters. In 2000, he returned to York to join the Department of Electronics.

David Grace received the MEng degree in electronic systems engineering and D.Phil degree from the University of York, UK in 1993 and 1999. His D.Phil thesis dealt with 'Distributed Dynamic Channel Assignment for the Wireless Environment.' Since 1994, he has been a member of the Communications Research Group at York, where he is now a Research Fellow. He has worked on a variety of research contracts including several from the former Defence Evaluation and Research Agency. Current research interests include radio resource management for broadband communications, particularly from high-altitude platform and terrestrial ad hoc networks. He is now a Principal Scientific Officer for CAPANINA, a major European Framework 6 project that is developing broadband communications from high-altitude platforms. He has been an Invited Speaker at several conferences and industrial locations in the fields of HAP systems. He is also a Nominated Researcher in the European NEWCOM Network of Excellence, and a Director of SkyLARC Technologies Ltd., a York based company, specializing in broadband communications from aerial platforms.